JACS
JOURNAL OF THE AMERICAN CHEMICAL SOCIETY
Communication
pubs.acs.org/JACS

# $Gd_{13}Fe_{10}C_{13}$: Indications of Fe–Fe Multiple Bonding Emerging from Chemical Frustration

Amelia B. Hadler and Daniel C. Fredrickson*

Department of Chemistry, University of Wisconsin-Madison, 1101 University Avenue, Madison, Wisconsin 53706, United States

Supporting Information

**ABSTRACT:** We report the synthesis and crystal structure of the carbide $Gd_{13}Fe_{10}C_{13}$. This compound adopts a new structure type that is remarkable for its "H"-shaped $C_2FeFeC_2$ units, which have some of the shortest Fe–Fe contacts known. A bonding analysis using DFT-calibrated Hückel calculations hints that Fe–Fe multiple bonding underlies these short distances. $Gd_{13}Fe_{10}C_{13}$ undergoes ferromagnetic ordering at ~55 K.

Intermetallic phases are one of the remaining frontiers of bonding interactions;[1] exploratory synthesis continues to reveal new phases that expand the mechanisms by which atoms stabilize their valence electrons. The carbides of intermetallics are particularly rich in this regard,[2] as their crystal structures must satisfy the competing requirements of metal–metal and metal–carbon bonding. While many intermetallics are built from packings of tetrahedra, carbon prefers to occupy larger spaces within metallic lattices, such as octahedral holes.[3] Intriguing bonding units often emerge from this frustration. Examples include the rare $C_3^{4-}$ anions first found in $Sc_3C_4$[2b,4] and later seen in $Ca_2LiC_3H$;[5] the isolated $Fe_4$ tetrahedra showing spin-glass behavior in $La_{21}Fe_8Sn_7C_{12}$;[6] and the planar $Fe_6$ clusters in $Er_{15}Fe_8C_{25}$.[7] $Er_{15}Fe_8C_{25}$ and other rare-earth–transition-metal–carbon (RE–TM–C) phases exhibit donor–acceptor TM–RE bonds similar to those seen in bimetallic molecular complexes.[2f,h]

Herein we describe hints of another bonding type that can emerge from the conflict of metal–metal and metal–carbon interactions: metal–metal multiple bonding. The crystal structure of the new phase $Gd_{13}Fe_{10}C_{13}$ (Figure 1) exhibits "H"-shaped $C_2FeFeC_2$ clusters whose Fe–Fe distances of 2.36–2.38 Å are among the shortest Fe–Fe contacts observed to date. Electronic structure calculations indicate that these short distances may reflect an Fe–Fe bond order near 2. Such multiple bonds between late first-row TM atoms are unusual within not only intermetallics and carbides but also coordination and organometallic chemistry.[8]

The rich structural chemistry of intermetallic carbides inspired us to pursue new phases in these systems through exploratory synthesis. The phase diagrams of many of the RE–TM–C systems provide useful launching points for such investigations. The phase diagram of the Gd–Fe–C system, for example, lists the six ternary phases $Gd_2Fe_{14}C$, $Gd_2Fe_{17}C_2$, $GdFe_2C_2$, $Gd_2Fe_2C_3$, $Gd_4Fe_4C_7$, and GdFeC, with the crystal structures of only the first two being known.[9,10]

In an attempt to synthesize one of these phases with an unknown structure, GdFeC, we arc-melted pellets of elemental Gd, Fe, and C and annealed them at 900 °C for 350 h. Crushing the resulting gray metallic ingots yielded crystals having a primitive trigonal cell with $a = 9.247(3)$ Å and $c = 23.713(8)$ Å.[11] Metric similarities to the 9.12 Å × 5.97 Å hexagonal cell reported for GdFeC as well as matches in some of the peaks in the powder X-ray diffraction patterns suggested that these were indeed crystals of the phase previously identified as GdFeC.

Structure solution and refinement using single-crystal X-ray diffraction revealed a new structure type. Application of the charge-flipping algorithm[12] yielded the positions of the metal atoms, and the C positions were subsequently found in the Fourier difference map, to give the stoichiometry $Gd_{13}Fe_{10}C_{13}$. The compound's structure is most easily described in terms of Fe-centered tricapped trigonal prisms (TTPs) of Gd atoms oriented along $c$ (Figure 1a). A side view of the structure shows

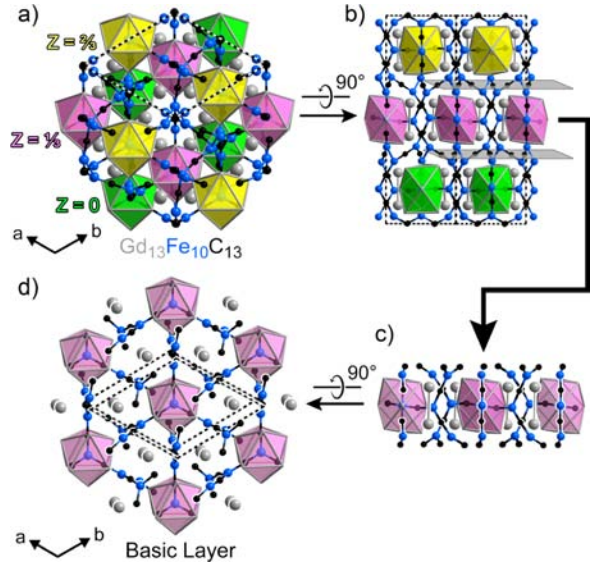


**Figure 1.** Crystal structure of $Gd_{13}Fe_{10}C_{13}$ (a) shown down $c$ to emphasize hexagonal layers of TTPs. (b) Rotation by 90° reveals an Fe–C matrix separating the prism layers. (c) A single layer is extracted and (d) rotated to show the contents of the basic layer.

that the TTPs are situated in layers stacked along $c$ (Figure 1b). Each layer can be divided geometrically into three components: TTPs, pairs of Gd atoms that trace honeycomb nets around each TTP, and an Fe–C network (Figure 1c,d).

**Received:** April 17, 2012
**Published:** June 7, 2012

   dx.doi.org/10.1021/ja3034944 | J. Am. Chem. Soc. 2012, 134, 10361–10364

The Gd forms a sublattice reminiscent of $Lu_8Te$ (Figure 2a), which itself adopts a variant of the $Fe_2P$ type.[13] As shown in

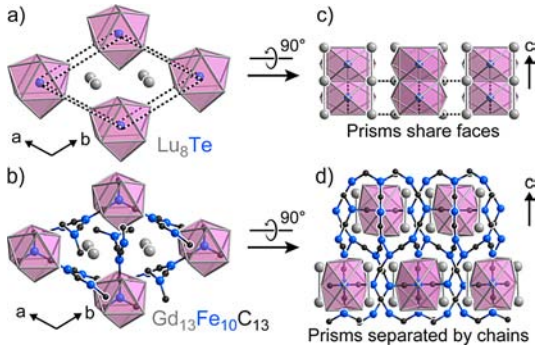


**Figure 2.** Comparison of (a) $Lu_8Te$ and (b) $Gd_{13}Fe_{10}C_{13}$. (c) Layers of TTPs share faces along *c* in $Lu_8Te$, while (d) the carbide matrix in $Gd_{13}Fe_{10}C_{13}$ prevents the prism layers from fusing.

Figure 2a,b, Te- or Fe-centered RE prisms and RE dumbbells form the same pattern in both phases. However, while the prisms in $Lu_8Te$ share triangular faces with those in the neighboring layers (Figure 2c), in $Gd_{13}Fe_{10}C_{13}$ an Fe−C network surrounds the prisms, preventing them from sharing faces and separating the layers (Figure 2d).

This intrusive carbide network can be imagined as extending from the Fe atoms centering the TTPs oriented along *c*. Each of these Fe sites is coordinated by three C atoms in a trigonal-planar Fe geometry (Figure 3a). Each of these carbons is bound to an

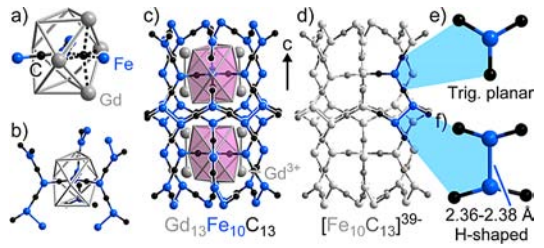


**Figure 3.** Fe−C network in $Gd_{13}Fe_{10}C_{13}$. (a) The square face of a TTP provides an octahedral site for a C atom. (b) Fe−C chains form from the prism-centering Fe atoms. (c) Prisms in adjacent layers are surrounded by the Fe−C matrix. (d) The $[Fe_{10}C_{13}]^{39-}$ network, shown in gray. (e) $FeC_3$ units are found within prism layers, while (f) $C_2FeFeC_2$ units appear at the interfaces between layers.

additional Fe, forming an octahedral C site at the Gd prism face and causing vertical elongation of the prism. The Fe atoms outside the prism center new $FeC_3$ planes perpendicular to the first (Figure 3b), yielding a paddlewheel-shaped fragment. Filling the coordination spheres of these C atoms and the resulting Fe atoms creates the carbide matrix shown in Figure 3c,d and leads to the formation of close Fe−Fe contacts at the interfaces of adjacent layers (Figure 3f).

As for many other carbide phases, the carbometalate concept provides a framework for understanding the bonding and electronic structure of this phase.[2d,f,14] The Gd atoms can be viewed *formally* as $Gd^{3+}$ cations, leaving the Fe and C atoms to form an anionic network with composition $[Fe_{10}C_{13}]^{39-}$ (Figure 3d).[15] Since there is no C−C bonding, all of the carbons are assigned as $C^{4-}$ anions, leaving 10 Fe atoms per formula unit to carry the remaining charge of +13, for an average Fe charge of +1.3. These 10 Fe atoms are distributed over sites with two types of coordination geometries (Figure 3e,f). Six of them, including those centering prisms, are coordinated in a trigonal plane to three C and no Fe atoms. The remaining four are paired into H-shaped $Fe_2C_4$ units in which each Fe is bound to two C atoms and one Fe atom, forming a local fragment reminiscent of a molecular Fe−Fe complex.

Two symmetry-inequivalent $C_2FeFeC_2$ units occur in the structure, both with surprisingly short Fe−Fe contacts: 2.362(2) Å (Fe3−Fe3) and 2.381(2) Å (Fe5−Fe5). Such short, localized Fe−Fe contacts are uncommon among both carbides and TM complexes. A few carbides have comparable Fe−Fe distances ($RE_2Fe_{17}C_{3-x}$, 2.37 Å; $RE_2Fe_{14}C$, 2.40 Å), but these contacts are part of a larger intermetallic framework and do not represent localized bonds.[16] The Fe−Fe bonds in carbides with isolated Fe clusters are significantly longer ($La_{21}Fe_8Sn_7C_{12}$, 2.55 Å; $Er_{15}Fe_8C_{26}$, 2.56 Å) and have bridging carbon atoms.[6,7] The Fe−Fe distances in $Gd_{13}Fe_{10}C_{13}$ are also short relative to those observed for TM complexes. Unsupported Fe−Fe distances usually lie in the range 2.68−3.14 Å,[17] but Lei et al.[18] recently reported the compound $(\eta^5\text{-}C_5H_5)(CO)_2FeFeAr$ [Ar = 3,5-$^i$Pr$_2$-2,6-(2,4,6-$^i$Pr$_3$C$_6$H$_2$)$_2$C$_6$H] containing an unbridged Fe−Fe bond with a length of 2.39 Å. Moving to shorter Fe−Fe bond distances appears to require the explicit constraints of bidentate ligands, as in the 2.20 Å Fe−Fe bond of the coordination complex $Fe_2$(*N*,*N*′-diphenylbenzamidinato)$_3$ reported by Cotton et al.[19]

As a first step in understanding the Fe−Fe interactions at these close contacts, we performed GGA−DFT band structure calculations on $Gd_{13}Fe_{10}C_{13}$ using the Vienna Ab Initio Simulation Package [see the Supporting Information (SI) for details].[20] As shown in Figure 4a, the non-spin-polarized

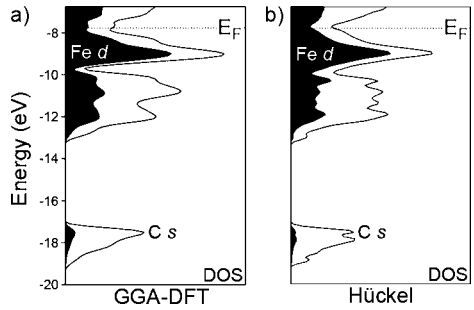


**Figure 4.** Non-spin-polarized DOS curves calculated for $Gd_{13}Fe_{10}C_{13}$ with (a) GGA−DFT and (b) a DFT-calibrated Hückel model. Partial DOS curves for Fe d states are shaded.

electronic density of states (DOS) distribution exhibits a pseudogap at the Fermi energy ($E_F$), a feature commonly associated with special stability of an intermetallic phase. The $E_F$ straddles larger DOS features that are relatively rich in Fe d character, consistent with our earlier assignment of the Fe charges as between +2 (Fe 3d$^6$) and +1 (Fe 3d$^7$). The pseudogap at the $E_F$ also suggests that there should be little contribution from Fe to any magnetic properties for this phase. Indeed, spin-polarized calculations (keeping the Gd 4f as a part of the pseudopotential core to make the calculations feasible) revealed little tendency for magnetic ordering on the Fe sites.

To explain these short Fe−Fe contacts, a simple Hückel model was parametrized against the DFT bands and projected DOS curves using our program eHtuner.[21] The resulting Hückel model shows strong quantitative agreement with the DFT band energies (with a root-mean-square deviation of 0.06 eV up to 1 eV above the $E_F$) and the DOS pseudogap at the $E_F$ (Figure 4b).


dx.doi.org/10.1021/ja3034944 | J. Am. Chem. Soc. 2012, 134, 10361−10364

In essence, then, the Hückel model allows for an orbital-based interpretation of the DFT electronic structure.

Crystal-orbital Hamiltonian populations (COHPs)[22] calculated using this Hückel model revealed that the DOS pseudogap separates bonding states from antibonding ones for the Fe−Fe, Fe−C, Fe−Gd, and Gd−C interactions, all of which are nearly optimized at the $E_F$ (see the SI). This supports a carbometalate view of the phase in which $Gd^{3+}$ cations stabilize Fe- and C-based energy levels (with contacts in the ranges 2.81−3.33 and 2.44−2.76 Å, respectively). Meanwhile, $C^{4-}$ anions form coordinate bonds with the Fe atoms (with lengths of 1.79−1.88 Å), and substantial Fe−Fe bonding occurs at the short contacts mentioned above.

What remain unresolved are the electron configurations of the Fe atoms. For the trigonal-planar Fe sites (Figure 3e), $\sigma$ interactions with the surrounding C atoms would destabilize two of the five d orbitals ($d_{xy}$ and $d_{x^2-y^2}$ using a local coordinate system in which $z$ is perpendicular to the trigonal plane). This would lead to a preferred electron configuration of low-spin $3d^6$ with a formal oxidation state of 2+, which is consistent with the lack of magnetic ordering at these sites observed in our spin-polarized calculations. Indeed, 2+ is a common oxidation state for Fe in trigonal-planar complexes.[23] As these account for six of the 10 Fe atoms in the formula unit, such bookkeeping leads us to the formal charges $(Gd^{3+})_{13}(Fe^{2+})_6(Fe^{0.25+})_4(C^{4-})_{13}$.

The remaining Fe atoms in the H-shaped units are then assigned a formal charge of 0.25, corresponding to a $3d^{7.75}$ electron configuration. From this point of view, the form of the Fe−Fe interactions between these sites can be readily interpreted using COHP analysis. The COHP curves for the $\sigma$ and two $\pi$ components of the Fe−Fe interactions at one of the $Fe_2$ units in the structure (between Fe5 sites) are shown in Figure 5 (the curves for the Fe3 site, which have comparable features, are given in the SI). The Fe−Fe $\sigma$ bonding is nearly optimized at the $E_F$, indicating that a full single bond exists between the two atoms (Figure 5a).

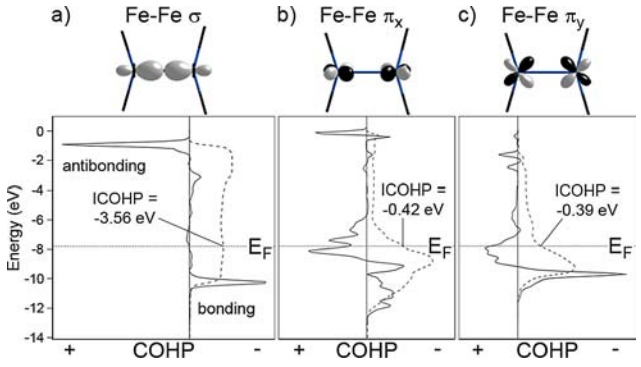


**Figure 5.** COHP analysis for (a) $\sigma$, (b) $\pi_x$, and (c) $\pi_y$ bonding in a $C_2FeFeC_2$ fragment of $Gd_{13}Fe_{10}C_{13}$. Integrated COHP (ICOHP) values are shown.

The two Fe−Fe $\pi$ interactions (Figure 5b,c) are less optimized; part of the antibonding region for both the $\pi_x$ and $\pi_y$ interactions lies below $E_F$. However, integration of the COHP curves revealed that in both cases, roughly half of the full stabilization energy possible from these $\pi$ interactions is retained at the $E_F$. Each $\pi$ interaction can thus be described as roughly a half bond, with the overall bond order approaching 2. The overall integrated $\pi$-bonding strength is ∼0.8 eV, a little less than a quarter of that associated with the $\sigma$ bond. This can be rationalized as arising from the weaker overlap for $\pi$ interactions and the significant torsion angles of 39.3−40.2° at the Fe−Fe contacts.

The character of the Fe−Fe interaction, the Fe $3d^{7.75}$ configuration, and the overall geometry of the $C_2Fe{=}FeC_2$ units can also be derived through a simple analogy to coordination chemistry. Within a $C_2Fe{=}FeC_2$ unit, each Fe atom is coordinated in a nearly linear fashion by two C atoms. Such linear coordination is common for complexes of $d^{10}$ cations, e.g. $Cu^+$, $Ag^+$, and $Au^+$.[24] Removing electrons from the d orbitals of such cations introduces the potential for metal−metal bonds to form upon dimerization of these linear units. Pairing of $d^9$ cations would lead to single bonds, $d^8$ cations to double bonds, and $d^7$ cations to triple bonds. For the $d^{7.75}$ configuration of the Fe atoms in the $C_2Fe{=}FeC_2$ fragments, a double bond would thus be expected. The population of $\pi$ antibonding states in the COHP curves indicates that this double bond emerges through the addition of electrons to the triple bond of the $d^7$−$d^7$ pair.

For reasons of computational feasibility, we have not yet considered the possibility of magnetic ordering on the Gd sublattice. Magnetization measurements (Figure 6) revealed that

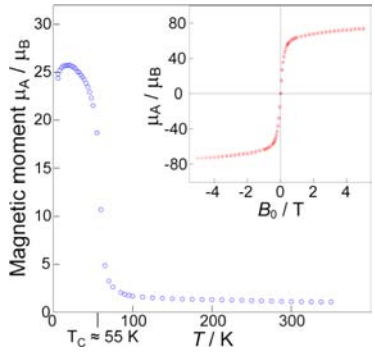


**Figure 6.** Magnetic property measurements on a sample containing $Gd_{13}Fe_{10}C_{13}$ as the major phase. Main figure: Magnetic moment as a function of temperature. Inset: Hysteresis curve measured at 6 K.

$Gd_{13}Fe_{10}C_{13}$ exhibits magnetic ordering below ∼55 K, yielding a soft ferromagnet with a saturation moment of ∼82 $\mu_B$ per formula unit at 6 K. The large size of this moment suggests that $Gd^{3+}$ cations are the major contributors. Significant deviations from Curie−Weiss behavior were observed, as is common for ferromagnetic materials containing multiple symmetry-inequivalent magnetic atoms.[25] Variability in the magnetic susceptibilities of samples above the Curie temperature and some residual ferromagnetism at higher temperatures can be attributed to ferromagnetic impurities.

In summary, $Gd_{13}Fe_{10}C_{13}$ crystallizes in a new carbide structure type consisting of $Fe_2P$-type layers of Gd TTPs interwoven with an Fe−C matrix. The carbide matrix features $C_2FeFeC_2$ units with Fe−Fe bond lengths of 2.36−2.38 Å, making this compound a unique expression of iron's chemistry. We have rationalized these contacts by evoking multiple bonds. However, multiple bonds between first-row TM atoms are challenging to model using DFT.[26] The Fe=Fe contacts in this phase are no exception: our attempts to optimize the geometry of this structure led to shrinkage of these contacts by ∼0.14 Å. Through continued experimental and computational characterization of this phase, we will investigate whether such deviations arise from limitations of the exchange−correlation functional or reflect spin ordering of the Fe atoms.


dx.doi.org/10.1021/ja3034944 | J. Am. Chem. Soc. 2012, 134, 10361−10364

The unusual Fe−Fe bonding in this phase is likely a consequence of the conflict between metal−metal and metal−carbon bonding that underpins complexity in intermetallic carbides. As mentioned above, these two bonding types have preferences for tetrahedral and simple periodic packing, respectively—packing modes known empirically to be incompatible.[27] Ternary metal carbides are faced with the issue of reconciling this incompatibility, a tension that can be interpreted as *chemical frustration*.[28] Further investigation of RE−TM−C systems is likely to reveal additional carbide structures with unusual bonding emerging from this conflict.

## ■ ASSOCIATED CONTENT

### Supporting Information

Experimental and computational methods, characterization data, and additional results. This material is available free of charge via the Internet at http://pubs.acs.org.

## ■ AUTHOR INFORMATION


### Corresponding Author

danny@chem.wisc.edu


### Notes

The authors declare no competing financial interest.

## ■ ACKNOWLEDGMENTS

We have enjoyed engaging discussions with Prof. John Berry regarding the difficulties of computational modeling of metal−metal bonds. We are also grateful to Dr. Ilia Guzei for collecting and processing single-crystal X-ray diffraction data, Rachel Selinsky for guidance with magnetic property measurements, and Drs. John Fournelle and Hiromi Konishi for assistance with EDS and powder X-ray diffraction measurements, respectively. Use of the Advanced Photon Source at Argonne National Laboratory was supported by the U.S. Department of Energy (DOE), Office of Science, Office of Basic Energy Sciences, under Contract DE-AC02-06CH11357. This research involved calculations using computer resources supported by NSF Grant CHE-0840494. We gratefully acknowledge financial support from the DOE Office of Science Early Career Program (DE-SC0003947) through the Office of Basic Energy Sciences, and from the University of Wisconsin through startup funds.

## ■ REFERENCES


(1) Nesper, R. *Angew. Chem., Int. Ed. Engl.* **1991**, *30*, 789.

(2) (a) Hoffmann, R.; Li, J.; Wheeler, R. A. *J. Am. Chem. Soc.* **1987**, *109*, 6600. (b) Hoffmann, R.; Meyer, H. J. *Z. Anorg. Allg. Chem.* **1992**, *607*, 57. (c) King, R. B. *J. Organomet. Chem.* **1997**, *536*, 7. (d) Pohlkamp, M. W.; Hoffmann, R. D.; Kotzyba, G.; Jeitschko, W. *J. Solid State Chem.* **2001**, *160*, 77. (e) Merschrod, E. F. S.; Courtney, A.; Hoffmann, R. *Z. Anorg. Allg. Chem.* **2002**, *628*, 2757. (f) Dashjav, E.; Kreiner, G.; Schnelle, W.; Wagner, F. R.; Kniep, R.; Jeitschko, W. *J. Solid State Chem.* **2007**, *180*, 636. (g) Rohrmoser, B.; Eickerling, G.; Presnitz, M.; Scherer, W.; Eyert, V.; Hoffmann, R. D.; Rodewald, U. C.; Vogt, C.; Pöttgen, R. *J. Am. Chem. Soc.* **2007**, *129*, 9356. (h) Dashjav, E.; Prots, Y.; Kreiner, G.; Schnelle, W.; Wagner, F. R.; Kniep, R. *J. Solid State Chem.* **2008**, *181*, 3121. (i) Vogt, C.; Hoffmann, R. D.; Rodewald, U. C.; Eickerling, G.; Presnitz, M.; Eyert, V.; Scherer, W.; Pöttgen, R. *Inorg. Chem.* **2009**, *48*, 6436. (j) Scherer, W.; Hauf, C.; Presnitz, M.; Scheidt, E. W.; Eickerling, G.; Eyert, V.; Hoffmann, R. D.; Rodewald, U. C.; Hammerschmidt, A.; Vogt, C.; Pöttgen, R. *Angew. Chem., Int. Ed.* **2010**, *49*, 1578.

(3) Yvon, K.; Parthé, E. *Acta Crystallogr.* **1970**, *B26*, 149.

(4) Pöttgen, R.; Jeitschko, W. *Inorg. Chem.* **1991**, *30*, 427.

(5) Lang, D. A.; Zaikina, J. V.; Lovingood, D. D.; Gedris, T. E.; Latturner, S. E. *J. Am. Chem. Soc.* **2010**, *132*, 17523.

(6) Benbow, E. M.; Dalal, N. S.; Latturner, S. E. *J. Am. Chem. Soc.* **2009**, *131*, 3349.

(7) Davaasuren, B.; Borrmann, H.; Dashjav, E.; Kreiner, G.; Widom, M.; Schnelle, W.; Wagner, F. R.; Kniep, R. *Angew. Chem., Int. Ed.* **2010**, *49*, 5687.

(8) *Multiple Bonds Between Metal Atoms*, 3rd ed.; Cotton, F. A., Murillo, C. A., Walton, R. A., Eds.; Springer: New York, 2005.

(9) Stadelmaier, H. H.; Park, H. K. *Z. Metallkd.* **1981**, *72*, 417.

(10) A $CeNiC_2$-type $GdFeC_2$ phase has also been reported. See: Jeitschko, W.; Gerss, M. H. *J. Less-Common Met.* **1986**, *116*, 147.

(11) Crystals of another phase having an Fe-centered orthorhombic cell with $a$ = 9.24 Å, $b$ = 16.02 Å, and $c$ = 31.73 Å were also obtained in some samples. The appearance of this phase was traced to brief exposure of the arc-melted samples to air before annealing. Carefully protecting the pellets from air exposure led to an enhanced yield of the trigonal phase and no observable formation of the orthorhombic one. Our characterization of this secondary phase is ongoing.

(12) (a) Oszlányi, G.; Sütő, A. *Acta Crystallogr.* **2004**, *A60*, 134. (b) Oszlányi, G.; Sütő, A. *Acta Crystallogr.* **2005**, *A61*, 147. (c) Palatinus, L.; Chapuis, G. *J. Appl. Crystallogr.* **2007**, *40*, 786.

(13) (a) Hendricks, S. B.; Kosting, P. R. *Z. Kristallogr., Kristallgeom., Kristallphys., Kristallchem.* **1930**, *74*, 511. (b) Chen, L.; Corbett, J. D. *J. Am. Chem. Soc.* **2003**, *125*, 7794.

(14) Dashjav, E.; Kreiner, G.; Schnelle, W.; Wagner, F. R.; Kniep, R. *Z. Anorg. Allg. Chem.* **2004**, *630*, 689.

(15) Formal charges are a bookkeeping tool and should not be mistaken as literal atomic charges. Bader charge analysis of the GGA−DFT results yielded Gd, Fe, and C atomic charges in the ranges +1.42 to +1.46, −0.20 to 0.05, and −1.44 to −1.35, respectively. Comparing these to the formal charges of $Gd^{3+}$, $Fe^{1.3+}$, and $C^{4-}$ indicates that relative to this ionic counting scheme, the C anions back-donate electrons to Fe and Gd and perhaps Fe back-donates to Gd as well.

(16) (a) Block, G.; Jeitschko, W. *Acta Crystallogr.* **1984**, *A40*, C239. (b) Marusin, E. P.; Bodak, O. I.; Tsokol, A. O.; Fundamensky, V. S. *Kristallografiya* **1985**, *30*, 581. (c) Block, G.; Jeitschko, W. *Inorg. Chem.* **1986**, *25*, 279. (d) Deboer, F. R.; Huang, Y. K.; Zhang, Z. D.; Demooij, D. B.; Buschow, K. H. J. *J. Magn. Magn. Mater.* **1988**, *72*, 167.

(17) (a) Putnik, C. F.; Welter, J. J.; Stucky, G. D.; D'Aniello, M. J.; Sosinsky, B. A.; Kirner, J. F.; Muetterties, E. L. *J. Am. Chem. Soc.* **1978**, *100*, 4107. (b) Deng, H. B.; Shore, S. G. *Inorg. Chem.* **1992**, *31*, 2289. (c) Hess, C. R.; Weyhermuller, T.; Bill, E.; Wieghardt, K. *Angew. Chem., Int. Ed.* **2009**, *48*, 3703.

(18) Lei, H.; Guo, J. D.; Fettinger, J. C.; Nagase, S.; Power, P. P. *J. Am. Chem. Soc.* **2010**, *132*, 17399.

(19) Cotton, F. A.; Daniels, L. M.; Falvello, L. R.; Matonic, J. H.; Murillo, C. A. *Inorg. Chim. Acta* **1997**, *256*, 269.

(20) (a) Blöchl, P. E. *Phys. Rev. B* **1994**, *50*, 17953. (b) Kresse, G.; Furthmüller, J. *Phys. Rev. B* **1996**, *54*, 11169. (c) Kresse, G.; Furthmüller, J. *Comput. Mater. Sci.* **1996**, *6*, 15. (d) Kresse, G.; Joubert, D. *Phys. Rev. B* **1999**, *59*, 1758.

(21) Stacey, T. E.; Fredrickson, D. C. *Dalton Trans.* **2012**, DOI: 10.1039/C2DT30298E.

(22) Dronskowski, R.; Blöchl, P. E. *J. Phys. Chem.* **1993**, *97*, 8617.

(23) Holland, P. L. *Acc. Chem. Res.* **2008**, *41*, 905.

(24) Greenwood, N. N.; Earnshaw, A. *Chemistry of the Elements*, 2nd ed.; Butterworth-Heinemann: Oxford, U.K., 1997.

(25) *Magnetic, Electrical and Optical Properties and Applications of Intermetallic Compounds*; Westbrook, J. H., Fleischer, R. L., Eds.; Wiley: West Sussex, U.K., 2000.

(26) Hall, M. B. *Polyhedron* **1987**, *6*, 679.

(27) Bernal, J. D. *Nature* **1959**, *183*, 141.

(28) Harris, N. A.; Hadler, A. B.; Fredrickson, D. C. *Z. Anorg. Allg. Chem.* **2011**, *637*, 1961.